Silica-Modifying Chemical Admixtures for Directed Zeolitization of Metakaolin-based Alkali-Activated Materials

J. Osio-Norgaard [a], *A.N. Aday* [b], *Xu Chen* [a], *S.L. Williams* [b], *J.P. Gevaudan* [a], *W.V. Srubar III* [a,b,†]

[a] Department of Civil, Environmental, and Architectural Engineering, [b] Materials Science and Engineering Program, University of Colorado Boulder, ECOT 441 UCB 428, Boulder, Colorado 80309-0428 USA, [†] Corresponding Author, T +1 303 492 2621, F +1 303 492 7317, E wsrubar@colorado.edu

Abstract

The effect of using trimethyladamantyl-ammonium hydroxide (TMAAOH) as a silica-modifying admixture to induce early-age mineralization during alkali-activation of metakaolin was investigated and reported herein. In all material formulations, the use of TMAAOH induced early-age mineralization, increased mixture stiffening in the fresh state, and lowered total heat of reaction. In activating solutions with silica moduli above unity (Ms >1.0), mineralogy results demonstrate that TMAAOH induces the nucleation and growth of metastable zeolitic phases, which correlated with increased permeability and increased plastic shrinkage of the paste. When TMAAOH was added to activating solutions with silica moduli near unity (Ms ~1.0), the controlled formation of crystalline, silica-rich faujasite was observed, which correlated with reduced permeability and lower plastic shrinkage. Together, these results demonstrate for the first time that silica-templating agents such as TMAAOH can be exploited in the deisgn of new chemical admixtures that directly influence the dynamics of zeolitization in alkali-activated materials.

Keywords: zeolites; mineralization; alkali-activated cements; rheology.

1.0 Introduction

Alkali-activated materials (AAMs) are a class of aluminosilicate cementitious materials produced by mixing aluminosilicate precursor powders (*e.g.*, fly ash, slag, metakaolin) with alkaline activating solutions (*e.g.*, NaOH, KOH). In general, AAMs can be classified by the cemenititous binder that composes them,

which varies depending on the calcium content available in the precursor [1]. Low-calcium AAM binders, which contain significantly lower calcium than conventional Portland cement (PC) [2–4], predominantly consist of a sodium-stabilized aluminosilicate hydrate framework (*i.e.*, N-A-S-H), although other alkalis can be used as charge-balancing cations. The short-range structure of NASH as a 3D aluminosilicate network has been recently studied and reported in [3].

The distinct chemistry of low-calcium AAMs has permitted their versatile utilization in a wide range of applications from construction [5], water filtration [6], soil stabilization [2], and nuclear waste containment [7], among others [8–10]. In the construction industry, AAMs offer a promising alternative to PC materials in certain applications due to lower cradle-to-gate CO_2 emissions, comparable mechanical properties, and, in some cases, improved durability [11,12].

1.1 Mineralogical Composition of AAMs

Understanding and controlling zeolite formation is a critical factor in developing durable microstructures in low-calcium AAMs. The combination of low-calcium aluminosilicate precursors (*e.g.*, metakaolin, clays) and both high-temperature and high-humidity curing conditions often induces the formation of zeolites [13]. The type, amount, and thermodynamic stability of zeolites that form can vary widely [14,15]. Zeolites are well known to affect the physical, mechanical, and durability properties of AAMs [15]. Zeolitization in AAMs has been linked with reduced porosity [13], potential chloride binding [16,17], mitigation of acid degradation [18], decreased efflorescence due to reduced sodium leaching [19], and heavy-metal and radioisotope immobilization [8,20,21].

Zeolite formtion in AAMs is identical to the sol-gel processes utilized to create synthetic zeolites. Both processes involve Si, Al, and alkali metals (*e.g.*, Na^+, K^+). Gevaudan *et al.* identified that both sodium-to-alumina ratio (Na:Al) and silica availability (*i.e.*, liquid vs. solid silica additions), along with environmental conditions during curing (*i.e.*, temperature, relative humidity) are critical factors that affect the formation of crystalline zeolite phases [13]. More specifically, high silica availability and high Na:Al ratios can lead to the early-age formation of faujasite zeolites in metakaolin-based AAM pastes [13]. Other

studies have confirmed that zeolite formation is favored at high alkali (*i.e.*, Na:Al > 1) and low silicon contents (*i.e.*, Si:Al ≤ 4), and when cured at elevated temperature and humidty [22,23].

In synthetic chemistry, zeolization can be precision-tailored using organic cationic templating agents (*e.g.*, quaternary ammonium compounds) [24–26]. Briefly, templating agents physicochemically interact with dissolved silica species and induce the nucleation and growth of zeolites in a templating fashion. The resulting zeolite mineralogy and metastability depends precisely on how oxide tetrahedra are structured into specific geometric arrangements [24].

These arrangements are primarily driven by the host-guest interactions between the organic cation and the silicate species that surround it. These interactions are influenced by the size and shape of the organic molecule, its hydrophobicity (or hydrophilicity), hydrothermal stability, and the rigidity or flexibility of its molecular bonds [24]. Diverse in their functionality, templating agents guide the stabilization of the aluminosilicate framework by initiating the formation—and ultimately dictating—the crystal size, morphology, and chemical composition of zeolites. A thorough review of the structure-directing agent phenomena can be found in [24].

1.2 Scope

The purpose of this study was to use an organic templating agent, namely trimethyladamantyl-ammonium hydroxide (TMAAOH), as a structure-directing chemical admixture for the express purpose of inducing early-age zeolitization in low-calcium AAMs. In addition to zeolitization, the associated effects on reaction kinetics, fresh-state behavior, and bulk material properties of AAM pastes were investigated and reported herein.

2.0 Materials and Methods

2.1 Materials

Metakaolin (MK) (MetaMax) was supplied by BASF (Georgia, USA). The chemical composition of the MK used in this study was previously reported by the authors in [13], and its X-ray diffractogram can be found in **Figure S1**. Reagent-grade sodium hydroxide (NaOH) pellets with >97% chemical purity and

sodium silicate (NaSi) M_s=2.5 (SiO_2 = 27 wt%, Na_2O = 11 wt%, H_2O = 62 wt%), were obtained from Sigma-Aldrich (St. Louis, MO, USA). TMAAOH was obtained from SACHEM (Austin, TX, USA). **Figure 1** shows the structure of TMAAOH. Lastly, ethanol (200 proof) was obtained from Fisher Scientific (Hampton, NH, USA).

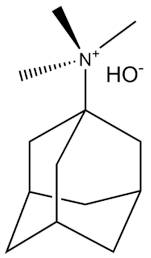

Figure 1: Chemical structure of TMAAOH.

2.2 Experimental Methods

2.2.1 Mixture Design & Sample Preparation

Twelve MK-based AAM paste mixtures were prepared by varying the Si:Al and Na:Al ratios according to the mixture design parameters listed in **Table 1**. A liquid-to-solid ratio of 2.0 was held constant across all samples. A TMAAOH:SiO_2 ratio of 0.02 was selected based on previous research reported in zeolite synthesis literature [27–30].

During preparation, the activating solutions were prepared by slowly dissolving the NaOH pellets in deionized (DI) water before adding sodium silicate. After having equilibrated for 24 hours at ambient conditions, the activating solution was manually mixed with MK then together with TMAAOH. The paste was then mechanically stirred for 3 minutes.

While some freshly mixed materials were tested for rheological (section 2.2.2) and calorimetric (section 2.2.3) behaviors, for all subsequent testing, the remaining materials were cast into 12x24mm HDPE cylindrical molds and cured under ambient humidity and pressure at 80 °C. After 7 days' curing, characterization experiments, including X-ray diffraction (XRD), plastic shrinkage, and permeable porosity, were conduced. Additional XRD patterns were also collected after 3 days of curing.

Table 1: Paste mixture formulations without and with TMAAOH addition. Silica modulus (Ms) is equivalent to the SiO_2/Na_2O molar ratio in the chemical activating solution. Si:Al, Na:Al, TMAAOH:SiO_2 refer to the molar ratios of the final mixture.

Mixture	MK (g)	NaSi (mL)	NaOH (g)	Na_2O/100g of Binder	Si:Al	Na:Al	Ms	TMAAOH:SiO_2	L/S
1	30	25	5	25.9	1.57	0.92	1.26	0	2.0
2								0.020	
3			10	38.8		1.37	0.84	0	
4								0.020	
5			15	51.7		1.84	0.63	0	
6								0.020	
7		45	5	36.1	2.03	1.28	1.62	0	
8								0.020	
9			10	49.0		1.74	1.19	0	
10								0.020	
11			15	61.9		2.21	0.94	0	
12								0.020	

2.2.2 Rheological Flow Curves

The rheological properties, namely yield stress and plastic viscosity, of MK-based AAM pastes, were determined with a MCR 301 rotational rheometer (Anton Paar, Graz, Austria). A 25 mm diameter stainless steel parallel plate geometry was used for all measurements, and the top plate was cross-hatched to minimize the influence of slip. The temperature was kept constant at 23 ± 0.1 °C, and the gap between the top and bottom plates was maintained at 1 mm. Prior to each test, approximately 700 µL of freshly mixed paste was transferred to the rheometer and subjected to pre-shearing at 50 s^{-1} for 30 seconds, followed by a 60 second rest period. The purpose of these pre-conditioning steps is to reduce the effects of shear history on the pastes and ensure reproducibility in testing [31]. The testing protocol consisted of linearly increasing the shear rate from 0 to 50 s^{-1} in 10 discrete intervals over a period of 100 seconds. At each shear rate, the shear stress was measured, and these data were used to generate flow curves. The pastes were modeled as Bingham plastic fluids [32]. Each flow curve was used to calculate yield stress and plastic viscosity according to the Bingham equation:

$$\tau = \tau_0 + \mu\dot{\gamma} \quad (1)$$

where τ is the shear stress, τ_0 is the yield stress (Pa), μ is the plastic viscosity (Pa-s), and $\dot{\gamma}$ is the shear rate (s^{-1}).

2.2.3 Isothermal Conduction Calorimetry (ICC)

A TAM Air 8-channel ICC (TA Instruments, New Castle, DE, USA) was used to evaluate the overall heat output of the fresh paste mixes and to identify any zeolitization-induced heat (as described in [7]). The ICC bath temperature was set to 80 °C and allowed to reach equilibrium over 3 days. Afterwards, an hour-long gain validation was performed. Initial and final baselines were measured for 1 hour to minimize signal noise. Around ten grams of freshly mixed paste was poured into glass ampules and placed in the calorimetry chamber at 80 °C. Heat flow data were collected for seven days for all mixtures, and data were normalized by the total mass.

2.2.4 X-Ray Diffraction (XRD)

Qualitative powder XRD analysis was performed with a Siemens D500 XRD (Bruker Corporation, Billerica, MA, USA). Samples were soaked in ethanol for 24 hours after curing to halt time-dependent chemical reactions. Subsequently, these were powdered and mixed with additional ethanol to form a slurry, which was then pipetted onto a single crystal silicon no-background plate. All samples were analyzed from 5 to 65° 2θ using Cu Kα radiation with a step size of 0.02° and a 2s dwell time per step. XRD was performed at 40kV and 30mA.

2.2.5 Hardened-State Properties: Shrinkage, and Permeable Porosity

Cylindrical specimens were removed from the curing chamber and demolded. Height and diameter measurements were taken using calipers. Dimensional plastic shrinkage was calculated by subtracting the diameter of the mold from the average diameter of the specimens after seven days of curing and determining a percent difference. After physical measurements were taken, samples were dewatered using an ethanol gradient to mitigate microcracking according to the following procedure. Samples were initially exposed to a 10% ethanol and water solution for one hour. Every subsequent hour the ethanol percentage was increased by 20%. Once samples were exposed to a 90% ethanol solution, they were exposed to a 100% ethanol solution overnight [13]. After samples were fully saturated, they were massed (M_{sat}) and placed in

an oven at 60 °C for 24 hours [33,34]. Subsequently, the dry masses (M_d) of the samples were obtained. Bulk density was determined by dividing M_d by the cylindrical volume (V_c) calculated from height and diameter measurements for each sample. Lastly, permeable porosity was calculated as the difference between M_{sat} and M_d normalized by the density of ethanol (0.789 g/cm^3) and divided by the sample cylindrical volume:

$$Porosity = \frac{(M_{sat} - M_d)}{0.789 * V_c} \quad (2)$$

3.0 Results and Analysis

3.1 Effect of TMAAOH on Rheological Properties

The yield stress and plastic viscosity of each paste formulation are reported in **Figure 2**. Data substantiate that the addition of TMAAOH increases both the yield stress and plastic viscosity of the pastes, especially at low Ms and high Si/Al ratios. For example, in the mix with Ms of 0.63 and Si:Al ratio of 1.57, addition of TMAAOH quadrupled the yield stress and doubled the viscosity. Such increases were even more substantial as the Si/Al ratio increased to 2.03, regardless of the Ms value.

The rapid increase in both yield stress and viscosity suggests that TMAAOH interacts chemically with the silicate species in the activating solutions. While a low-Ms value (*i.e.,* with high alkalinity) induces rapid dissolution of the precursor and creates (alumino)silicate oligomers in solution [35–38], a high Si/Al ratio also favors production of the oligomers [39,40]. In either case, these negatively-charged oligomers are stabilized by the cationic sites of TMAAOH, the process known as the "templating effect" of organic molecules. As a consequence, the stabilization of oligomers stiffens the mixture and yields discernible increases in both the yield stress and viscosity of AAM pastes [41,42]. Thus, fresh state evidence indicates that TMAAOH induces a templating—and stiffening—effect during alkali activation of MK as it does during pure zeolite synthesis [43].

This study, in line with previous research, shows that TMAAOH-free MK pastes have yield stresses < 2 Pa (**Figure 2**) [37,44]. The addition of TMAAOH increases the yield stress of all Si:Al=2.0 samples from ~2 Pa to between 11-16 Pa (**Figure 2**).

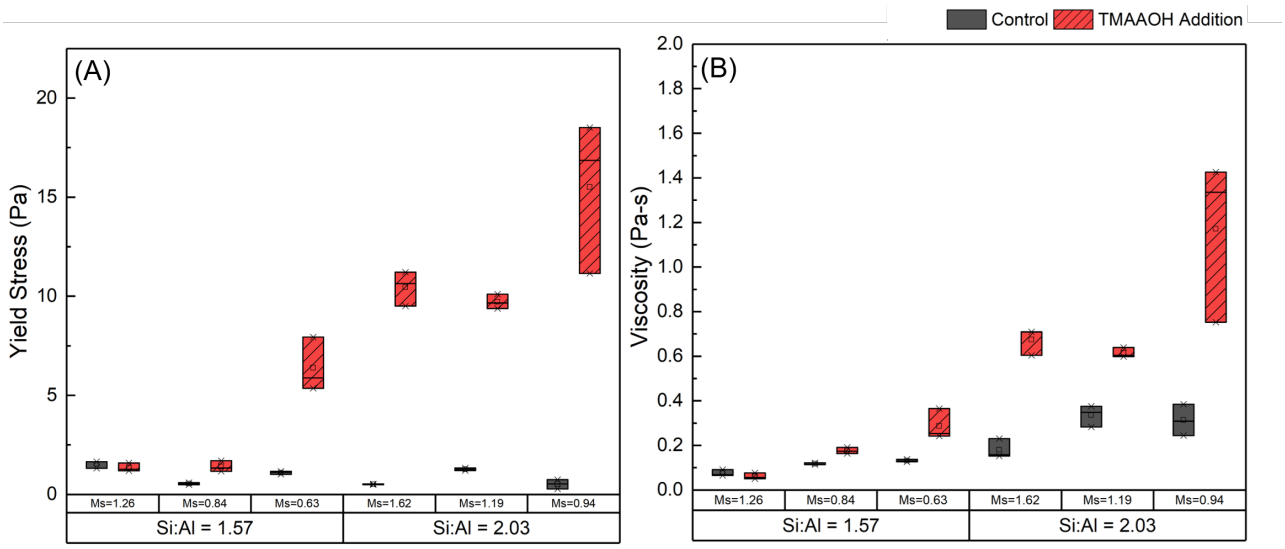

Figure 2. (a) Yield stress and (b) plastic viscosity of MK-based AAM pastes without and with TMAAOH addition. Error bars represent ± one standard deviation (n=3).

3.2 Effect of TMAAOH on Mineralogy

Figure 3 and **Figure 4** present the mineralogical data obtained from the AAMs at Si:Al ratios of 1.57 and 2.03, respectively. It is evident that TMAAOH induced the formation of zeolites, such as faujasite (Si:Al = 2.3), chabazite (Si:Al = 2.1), and sodalite (Si:Al = 1.0), in comparison to non-supplemented controls [45–47]. As explained previously, TMAAOH templates local silica oligomers during alkali activation, which mimics the direct *in situ* crystallization methods for pure zeolite synthesis [24,48]. In this methodology, aluminosilicate gels, produced during alkali-activation, precipitate onto the organic template, which facilitates zeolite nucleation and growth [30]. Mechanistically speaking, TMAAOH catalytically reduces the thermodynamic activation energy to nucleate zeolites [24,29,49–51].

The zeolite types induced by the TMAAOH were silicon-rich faujasite and chabazite or aluminum-rich sodalite. Silicon-rich chabazite has been previously identified in MK and fly ash activated materials, however, extended-time studies (>84 days) have revealed that this zeolite phase is largely metastable [52] and will thermodynamically transition to other more stable zeolitic phases over time. The identified zeolites were found to depend on the Ms value of the activating solution as discussed in the following section.

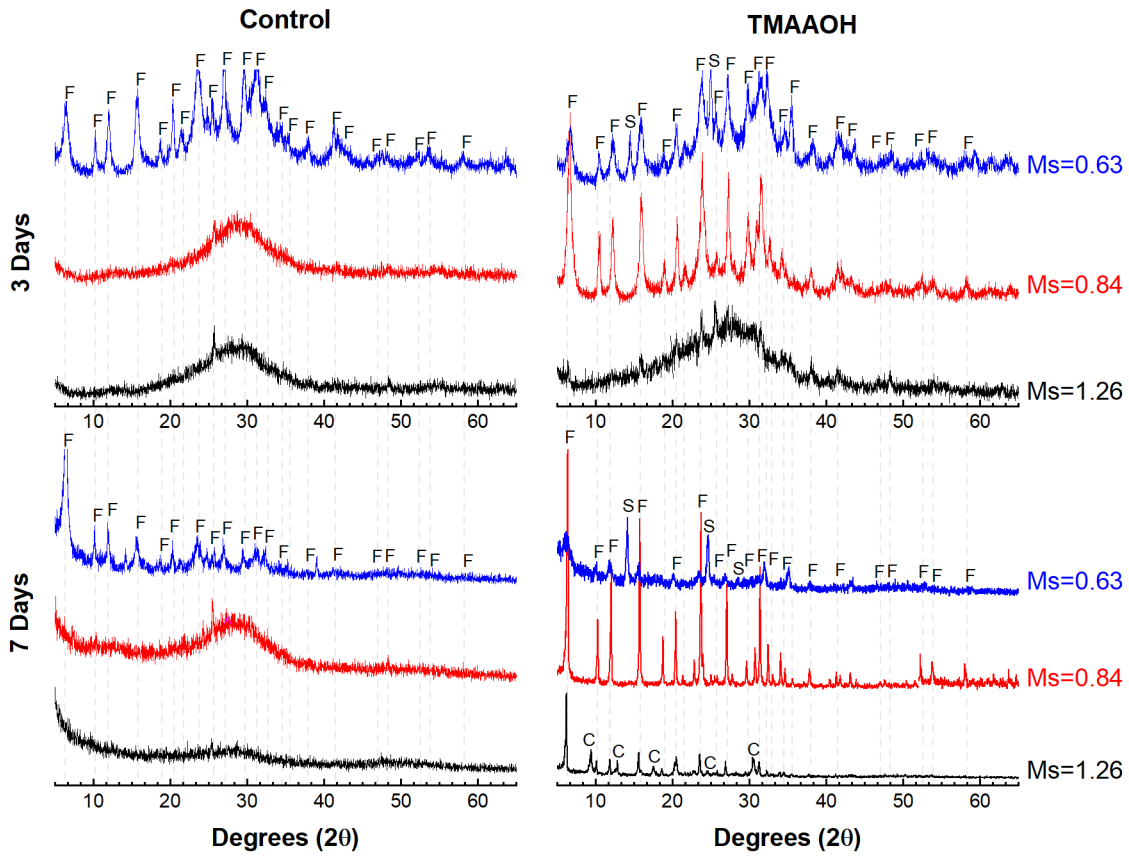

Figure 3. X-Ray diffractograms of alkali-activated MK with Si:Al=1.57 at three (72 hours) and seven days (168 hours). C=Chabazite (*Si:Al = 2.1,* PDF 00-019-1178), F=faujasite (*Si:Al = 2.3,* PDF 00-012-0228), S = Sodalite Octahydrate (Si:Al = 1.0).

In activating solutions with silica moduli (Ms) higher than unity (>1.0), zeolite nucleation induced by TMAAOH favored silicon-rich minerals (*i.e.*, chabazite and faujasite). From **Figure 3** and **Figure 4**, it is evident that chabazite only forms after 7 days of curing in formulations with: (Si:Al = 2.0, Na:Al = 1.28), (Si:Al = 1.57, Na:Al = 0.91), and (Si:Al = 2.0, Na:Al = 1.38). These formulations have Ms values of 1.19, 1.26, and 1.62, respectively. It is well known that a Ms >1.0 promotes the formation of silica oligomers (*e.g.*, bridged cyclic tetramers, cyclic trimers, and linear trimers), which would yield better interaction with TMAAOH, as previously explained [39,40]. Besides interacting with the initial activating solution, the TMAAOH, with a lower ratio of charge per molecule size compared to Na^{+}, more likely stabilizes higher Si:Al aluminosilicates that possess a lower number of balancing negative charges [53]. During alkali-

activation, nucleation of these zeolites results from precipitated aluminosilicate gels similar to the 'gel 2' described in [54] (Si:Al ~2.0).

In contrast, the use of activating solutions with Ms lower than unity (Ms = 0.63) yields the formation of low Si:Al zeolites as verified by the formation of sodalite in formulations with (Si:Al = 2.0, Na:Al = 1.74). In these low-Ms activating solutions, the majority of silica species are monomers with remnant dimers and trimers [38–40,55]. These species are highly reactive and favor the rapid formation of low-Si:Al gels termed "gel 1" [39,54]. Moreover, the formation of sodalite zeolites may also be due to an out-competition of Na^+ over the $TMAA^+$ cations for sorption surface sites on precursor particles, as seen in a similar system with combined organic-inorganic cations [56]. XRD data confirm TMAAOH's utility in inducing early-age mineralization in AAMs [57,58].

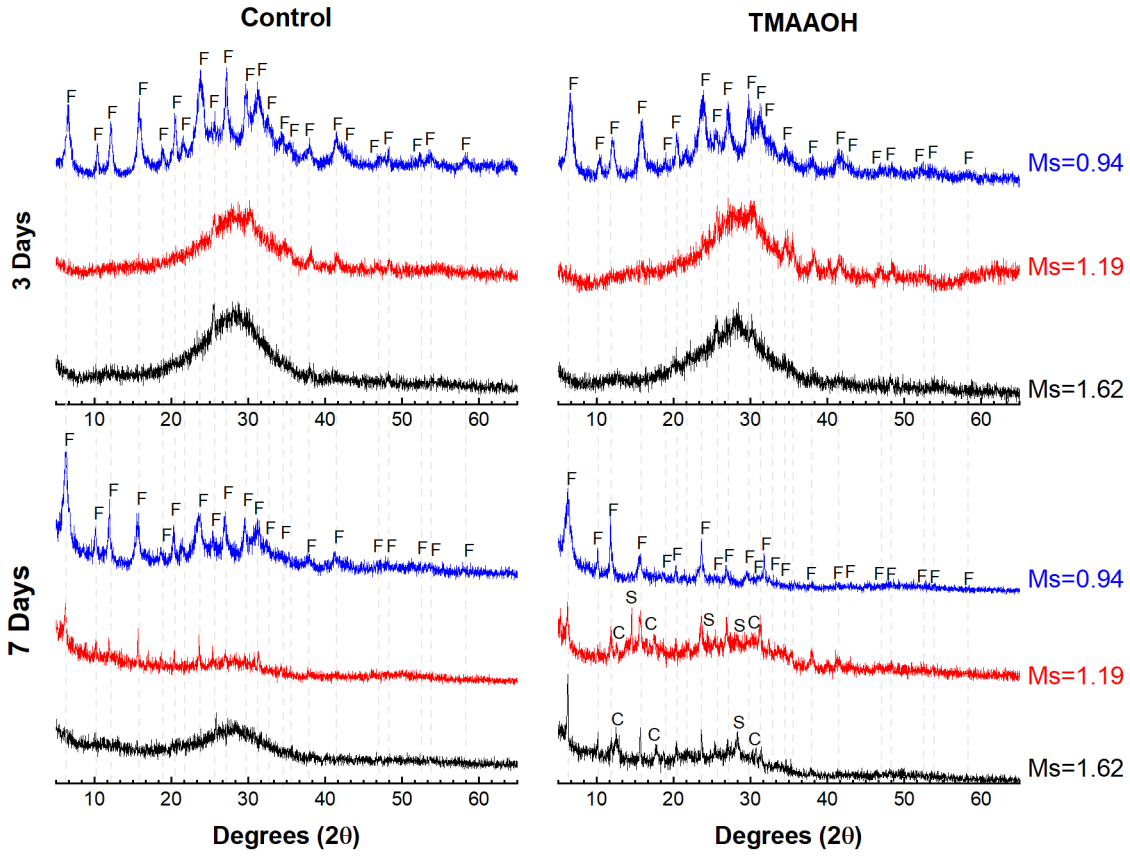

Figure 4. X-Ray diffractograms of alkali-activated MK with Si:Al=2.0 at three (72 hours) and seven days (168 hours). C=chabazite (*Si:Al = 2.1,* PDF 00-019-1178), F=faujasite (*Si:Al = 2.3,* PDF 00-012-0228), S = Sodalite Octahydrate (Si:Al = 1.0).

3.3 Effect of TMAAOH on Reaction Kinetics

Figure 5 shows the heat evolution of the MK pastes without and with TMAAOH addition. The exothermic peaks exhibited in this figure correlate with mineral formation (see **Figure 3** and **Figure 4**) and provide direct evidence of mineralization thermodynamics occuring in these samples. For example, (Si:Al = 1.57, Na:Al = 0.91) formulations with TMAAOH and Ms = 1.26 exhbit higher heat evolution during alkali activation (100.7 J/g) and reach peak heat at earlier timepoints (~30 hours earlier). These results correlate well with XRD, which substantiate that TMAAOH addition in these samples increases the degree of mineralization (content of minerals) by forming silicon-rich zeolites, such as faujasite and chabazite.

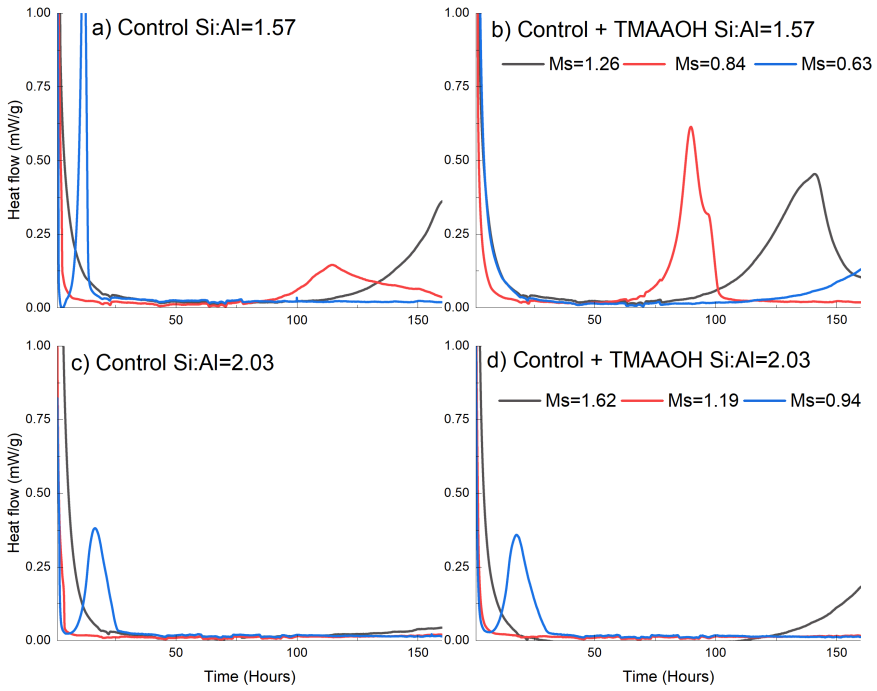

Figure 5. Normalized heat flow curves of alkali-activated MK paste formulations with Si:Al=1.57 and Si:Al=2.03, as indicated within the figure (168 hours).

As observed in **Figure 5b**, formulations with TMAOOH at Si:Al=1.57 and increasing Na:Al ratios resulted in rapid early-age mineralization. For example, control samples (**Figure 5a**) with a Na:Al=1.84 displayed two exothermic peaks before 3 days, which correlated with faujasite formation in the first 10 hours as observed *via* XRD. Alternatively, samples with TMAOOH exhibit one initial peak and the formation of both faujasite and sodalite (**Figure 3**). Hence, only in the presence of TMAAOH and a low Ms, zeolite nucleation is accelerated and occurs in the first few hours upon activation. This finding is consistent with the *in situ* crystallization mechanisms of 'gel 1' explained earlier. While the formation of low Si:Al 'gel 1' proceeds rapidly [59,60], evidence obtained herein indicated that TMAAOH futher accelerated this process *via* zeolitization in this sample. Similar TMAAOH-induced acceleration was observed for formulations of the same silica content and lower Na:Al ratios.

Samples with a Si:Al=2.03 (**Figure 5c** and **Figure 5d**) exhibited similar behavior regardless of TMAAOH addition. Further analysis of the total heat released from these samples is summarized in **Table 2.** The results indicate that a slight increase (8%) in total heat at 7 days is observed for formulations with TMAAOH and activating solutions with Ms values near unity (Si:Al =2.0, Na:Al = 2.2). An increase in total heat, as discussed previously, indicates a larger extent of mineral (*i.e.*, faujasite) formation. Contrastingly, formulations with the same silica content and TMAAOH but activated with solutions of higher Ms yield up to 35% lower heat of reaction. Reductions in the heat flow produced during alkali activation and curing are beneficial in regard to reduced thermal shrinkage.

Table 2. Total heat flow from isothermal calorimetry data for all AAM formulations.

Ms	**0.63**		**0.84**		**0.94**	
Na/Al	1.84		1.37		2.2	
Si/Al	1.57		1.57		2.03	
Sample	Control	TMAAOH	Control	TMAAOH	Control	TMAAOH
Heat (J/g): 3 days	109.6	67.5	89.3	84.3	73.6	81
Heat (J/g): 7 days)	116.6	80.5	111.7	117.6	79	85.7
Ms	**1.19**		**1.26**		**1.62**	

Na/Al Si/Al	1.74 2.03		0.91 1.57		1.28 2.03	
Sample	Control	TMAAOH	Control	TMAAOH	Control	TMAAOH
Heat (J/g): 3 days	75.1	74.2	54.9	47	81.3	45.9
Heat (J/g): 7 days)	80	78.7	83.6	100.7	88.7	56.5

3.4 Effect of TMAAOH on Permeable Porosity and Plastic Shrinkage

The permeable porosities of samples without and with TMAAOH are shown in **Figure 6**. As previously discussed, formulations with Ms >1.0, TMAAOH induced the formation of chabazite, a metastable phase (see **Figure 3** and **Figure 4**). As expected from the authors' previous work [13], the formation of this metastable phase leads to an average increase in the permeable porosity (see **Figure 6**). For example, formulations Ms=1.62 and Ms=1.19 form chabazite and exhibit an increase in mean permeable porosity of 10% at 7 days. Interestingly, chabazite in Ms=1.26 samples do not reveal significant changes in mean permeable porosity, but a larger data variance is observed. In addition, Ms=0.63 samples, which were activated with the lowest Ms activating solution, demonstrated rapid mineral formation (**Figure 5**), which led to an an increase (7%) in the mean permeable porosity after seven days of curing.

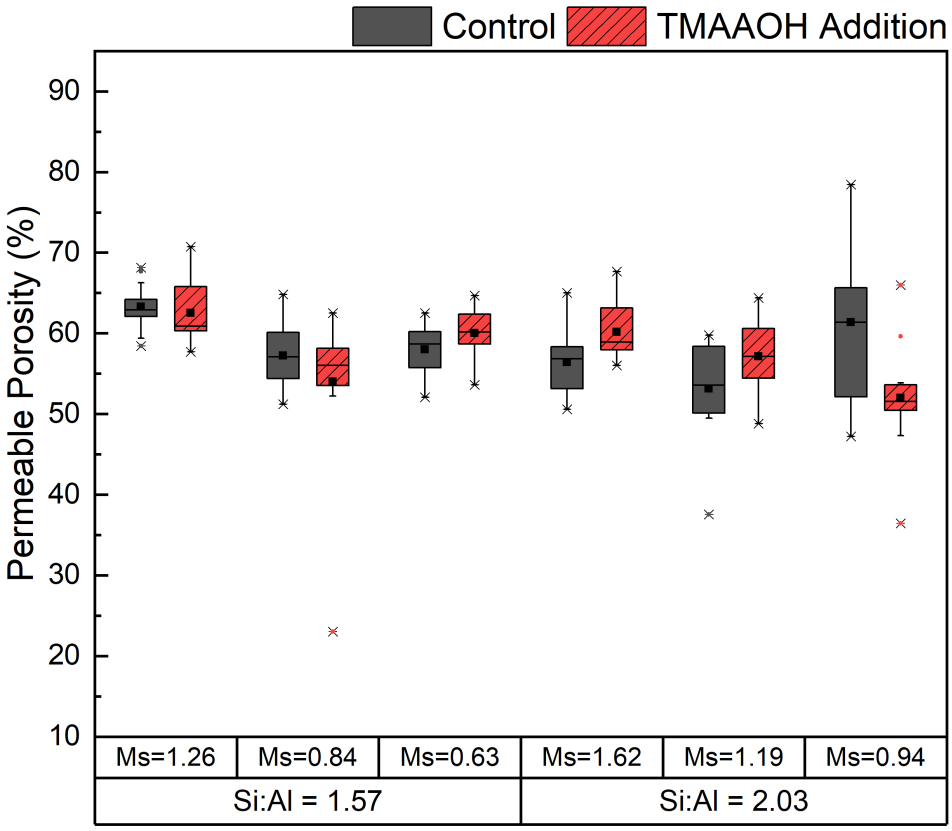

Figure 6. Permeable porosity of MK pastes without and with TMAAOH addition after 7 days of curing, n = 9.

AAMs activated with TMAAOH and Ms near unity demonstrate an equal or lower permeable porosity as those without TMAAOH (**Figure 6**). This lower permeable porosity is attributable to a greater extent of faujasite formation. Early-age faujasite mineralization was confirmed *via* XRD (**Figure 3** and **Figure 4**) and evidenced in calorimetry measurements (**Figure 5** and **Table 2**). More specifically, TMAAOH addition reduced the mean permeable porosity in mixtures with Ms=0.84 and in mixtures with Ms = 0.94) 1% and 16%, respectively (see **Figure 6**). As explained by the authors in [13] and further confirmed by [19], the controlled growth of a silicon-rich zeolite (*i.e.*, faujasite) lowers the permeable porosity in low-calcium AAMs. Interestingly, these reductions in permeable porosity seem to be unrelated to the framework density of the zeolites formed. Although chabazite (15.1T/1000A) and sodalite (16.7T/1000A) have greater framework densities than faujasite (13.3T/1000A) and are thereby less porous, the mixes in which these

zeolites developed exhibit a greater permeable porosity than those where exclusively faujasite formed. This perhaps indicates that the time at which the zeolites develop has a greater influence on permeable porosity than the type of zeolite formed. These results provide a limited picture of the effect of TMAAOH on the porosity and microstructure of AAMs. The high water content of the samples and the test's inability to assess the mesoporosity of the formed zeolites indicate that further testing should be performed to observe changes in other meaningful properties such as pore size distribution. The permeable porosity results, however, do serve as a proxy measurement to initially understand some of the potential microstructural changes that occur with TMAAOH addition.

Figure 7 shows the plastic shrinkage measurements of all pastes. In line with permeable porosity results, the plastic shrinkage of AAMs is lowered when TMAAOH is included as a chemical admixture with activating solutions with a Ms ~1.0. In samples without TMAAOH, there is an expected increase in shrinkage with increases in both Na:Al and Si:Al ratios [61]. Different shrinkage mechanisms apply to TMAAOH-supplemented samples. When TMAAOH is added to AAM mixtures, the rapid nucleation of some stable zeolites (*e.g.*, sodalite) and metastable phases (*i.e.*, chabazite) can result in the formation of silicon-rich N-A-S-H binders susceptible to shrinkage [13]. As previously noted, these mineral dynamics are a result of Ms > 1.0 in the activating solutions. At Ms ~1.0, plastic shrinkage is decreased by 20%, due to a stable increase of faujasite forming in these samples, as evidenced by XRD and isothermal calorimetry. The measurements of both permeable porosity and plastic shrinkage provide an initial picture of the impact TMAAOH has on the hardened state properties of these AAM mixtures. However, further studies should be conducted to elucidate the impact TMAAOH (or other SDAs) have on the various types of shrinkage experienced by these materials (*e.g.* drying shrinkage). Taken together, these results illustrate the potencial efficacy of using TMAAOH in combination with activating solutions with Ms ~1.0 to achieve a denser microstructure and lower permeable porosity.

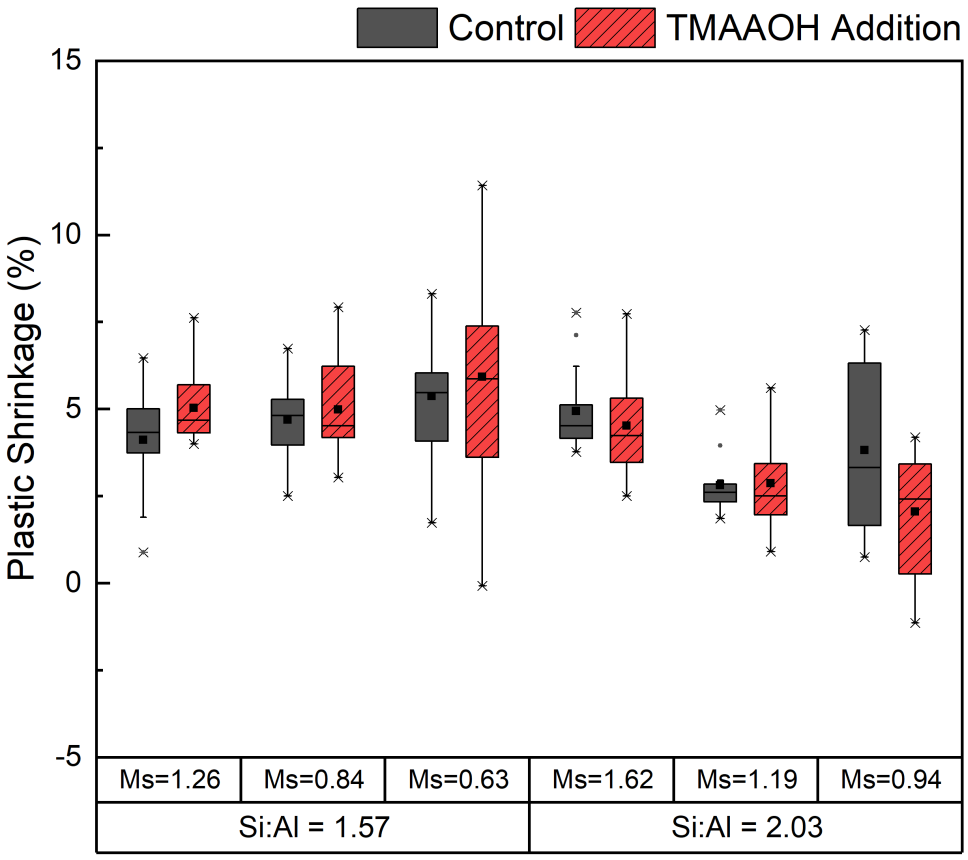

Figure 7. Plastic shrinkage of alkali-activated MK paste formulations without and with TMAAOH addition after 7 days of curing (n = 9).

4. Significance and Future Research

By merging the fields of artificial zeolite synthesis with AAMs, this proof of concept work demonstrates that organic templating agents can be used to manipulate reaction kinetics, early-age microstructural development, and both fresh- and hardened-state properties of AAMs. Incorporating templating agents as novel AAM admixtures could increase their tailorability and lead to performance improvements. For example, the controlled development of early-age faujasite in this study could lead to beneficial mineralogical and microstructural changes. We showed that, when templating agents are utilized in activating solutions with a Ms near unity, the early-age formation of faujasite can reduce the volume of

permeable pores – a critical factor that reduces chloride diffusivity and, in general, improves long-term durability [13]. Moreover, it is suspected that faujasite and chabazite themselves have the potential to affect chloride transport by increasing chloride binding [62], which could lead to increased chloride binding within these microstructures. Beyond the zeolites templated in this study, other zeolites like 13X FAU, a well-known CO_2 sorbent [63], could be templated to increase CO_2 capture in geopolymer pastes. The potential for process-structure-property exploration into how various templating agents and their chemistries interact with geopolymerization to mineralize the desired zeolites provides a fruitful new area of research related to *mineralization* or *zeolitization admixture* technology.

Furthermore, the work herein demonstrated that templating agents could be developed into a new class of *viscosity-modifying admixtures* for geopolymer pastes. Our results show that the incorporation of TMAAOH increased yield stresses of MK geopolymer pastes regardless of Si:Al or Na:Al ratio. Future research is needed, however, to test a suite of chemically tailored viscosity modifying admixtures, which could be developed using one or more various templating agents in combination. Developing various viscosity-modifying admixtures would widen the range of AAM applications, especially those involving additive manufacturing in 3D concrete printing.

It is important to note that this work has some inherent limitations. A limited number of mixes were explored, all with high liquid to solids ratios, which generally led to high porosities. Additional research would be needed to design and optimize mixtures with SDAs for specific applications to achieve target physical and mechanical properties and acceptable durability performance.

5.0 Conclusion

In this study, we demonstrated that TMAAOH could be utilized as a new chemical admixture in AAMs to induce the early-age formation of silicon-rich zeolites. TMAAOH is observed to directly affect the polycondensation of silica species during alkali-activation, which manifested as quantifiable increases in yield stress and plastic viscosity of the mixtures. Such increases were observed to be much higher for

mixtures activated with silica moduli near unity (Ms ~1.0). This observation indicates that TMAAOH will preferentially interface with short-chained silica oligomer species.

The enhanced formation of faujasite *via* TMAAOH templating is attributable to its capability of nucleating a high Si:Al framework. The results suggest that TMAAOH follows a direct *in situ* crystallization methodology, which favors the precipitation of aluminosilicate gels and consequent zeolite nucleation. When TMAAOH was utilized with Ms above unity (Ms >1.0), samples were observed to form faujasite and chabazite (**Figure 2** and **Figure 3**), two well-known silicon-rich zeolites. The formation of chabazite, a metastable zeolite, led to increases in permeable porosity and plastic shrinkage. Contrastingly, the controlled formation of faujasite with activating solutions having a Ms ~1.0 and TMAAOH resulted in reduced permeable porosity and plastic shrinkage. Lastly, the total heat of reaction for samples including TMAAOH was lower than their control formulations.

The results presented herein indicate the need for further investigation into the potential for structure-directing agents to serve as potential mineralization or zeolitization admixtures to tailor the fresh- and hardened-state properties of AAMs. Furthermore, this study highlights the possibility of investigating other templating agents for material-modifying properties, as well as an ability to induce the formation of useful zeolites. For example, this new class of chemical admixtures could promote the formation of functional zeolites in AACs that further densify the microstructure, increase chloride binding, reduce chloride transport, and enhance *in situ* CO_2 sequestration.

6.0 Acknowledgments

This research was made possible by the Department of Civil, Environmental, and Architectural Engineering, the College of Engineering and Applied Sciences, and the Living Materials Laboratory (LMLab) at the University of Colorado Boulder, with financial support from the National Science Foundation (NSF) (Award No. CBET-1604457), the NSF Graduate Research Fellowship Program, and the Advanced Research Projects Agency-Energy (Award Number: DE-AR0001145). Dr. J.P. Gevaudan's participation in this study was supported by the European Union's Horizon 2020 research and innovation programme under the Marie Skłodowska-Curie grant agreement No. 839436. Additionally, the authors

would like to thank the United States Geological Survey, BASF for the donation of MK from BASF, and SACHEM for donating the adamantium hydroxide. This work represents the views of the authors and not necessarily those of the sponsors.

7.0 References

[1] M. Juenger, F. Winnefeld, J.L. Provis, J. Ideker, Advances in alternative cementitious binders, Cem. Concr. Res. 41 (2011) 1232–1243.

[2] J.P. Gevaudan, J. Osio-Norgaard, W. V. Srubar, Alternative Cements: Recent Developments and Future Directions, in: AEI 2019, American Society of Civil Engineers, Reston, VA, 2019: pp. 294–308. https://doi.org/10.1061/9780784482261.035.

[3] B. Walkley, G.J. Rees, R. San Nicolas, J.S.J. van Deventer, J. V Hanna, J.L. Provis, A New Structural Model of Sodium Aluminosilicate Gels and the Role of Charge Balancing Extra-Framework Al, J. Phys. Chem. C. 4 (2018) acs.jpcc.8b00259. https://doi.org/10.1021/acs.jpcc.8b00259.

[4] P. Duxson, A. Fernández-Jiménez, J.L. Provis, G.C. Lukey, A. Palomo, J.S.J. Van Deventer, Geopolymer technology: The current state of the art, J. Mater. Sci. 42 (2007) 2917–2933. https://doi.org/10.1007/s10853-006-0637-z.

[5] P. Duxson, J.L. Provis, G.C. Lukey, J.S.J. van Deventer, The role of inorganic polymer technology in the development of "green concrete," Cem. Concr. Res. 37 (2007) 1590–1597. https://doi.org/10.1016/j.cemconres.2007.08.018.

[6] E. Ofer-Rozovsky, M. Arbel Haddad, G. Bar Nes, A. Katz, The formation of crystalline phases in metakaolin-based geopolymers in the presence of sodium nitrate, J. Mater. Sci. 51 (2016) 4795–4814. https://doi.org/10.1007/s10853-016-9767-0.

[7] S.A. Walling, S.A. Bernal, L.J. Gardner, H. Kinoshita, J.L. Provis, Phase Formation and Evolution in Mg(OH) 2 –Zeolite Cements, Ind. Eng. Chem. Res. 57 (2018) 2105–2113. https://doi.org/10.1021/acs.iecr.7b04201.

[8] Z. Xu, Z. Jiang, D. Wu, X. Peng, Y. Xu, N. Li, Y. Qi, P. Li, Immobilization of strontium-loaded zeolite A by metakaolin based-geopolymer, Ceram. Int. 43 (2017) 4434–4439. https://doi.org/10.1016/J.CERAMINT.2016.12.092.

[9] T.J. Kirkpatrick, R.E. Weyers, C.M. Anderson-Cook, M.M. Sprinkel, Immobilization of Cr6+, Cd2+, Zn2+ and Pb2+ in alkali-activated slag binders, Cem. Concr. Res. 32 (2002) 1971–1979. https://doi.org/10.1016/S0008-8846(02)00904-3.

[10] S. Xiaodong, Y. Sheng, W. Xuequan, T. Mingshu, Y. Liji, Immobilization of stimulated high level wastes into AASC waste form, Cem. Concr. Res. 24 (1994) 133–138. https://doi.org/10.1016/0008-8846(94)90094-9.

[11] J.L. Provis, A. Palomo, Advances in understanding alkali-activated materials, Cem. Concr. Res. 78 (2015) 110–125. https://doi.org/10.1016/j.cemconres.2015.04.013.

[12] S.A. Bernal, J.L. Provis, Durability of alkali-activated materials: Progress and perspectives, J. Am. Ceram. Soc. 97 (2014) 997–1008. https://doi.org/10.1111/jace.12831.

[13] J.P. Gevaudan, K.M. Campbell, T.J. Kane, R.K. Shoemaker, W. V. Srubar, Mineralization dynamics of metakaolin-based alkali-activated cements, Cem. Concr. Res. 94 (2017) 1–12. https://doi.org/10.1016/j.cemconres.2017.01.001.

[14] G. Cruciani, Zeolites upon heating: Factors governing their thermal stability and structural changes, J. Phys. Chem. Solids. 67 (2006) 1973–1994.

[15] J.L. Provis, G.C. Lukey, J.S.J. Van Deventer, Do geopolymers actually contain nanocrystalline zeolites? a reexamination of existing results, Chem. Mater. 17 (2005) 3075–3085. https://doi.org/10.1021/cm050230i.
[16] Y. Jun, S. Yoon, J. Oh, A Comparison Study for Chloride-Binding Capacity between Alkali-Activated Fly Ash and Slag in the Use of Seawater, Appl. Sci. 7 (2017) 971. https://doi.org/10.3390/app7100971.
[17] J. Osio-Norgaard, J.P. Gevaudan, W. V. Srubar, A review of chloride transport in alkali-activated cement paste, mortar, and concrete, Constr. Build. Mater. 186 (2018) 191–206. https://doi.org/10.1016/j.conbuildmat.2018.07.119.
[18] P. Sturm, G.J.G. Gluth, C. Jäger, H.J.H. Brouwers, H.C. Kühne, Sulfuric acid resistance of one-part alkali-activated mortars, Cem. Concr. Res. 109 (2018) 54–63. https://doi.org/10.1016/j.cemconres.2018.04.009.
[19] F. Pacheco-Torgal, Z. Abdollahnejad, A.F. Camões, M. Jamshidi, Y. Ding, Durability of alkali-activated binders: A clear advantage over Portland cement or an unproven issue?, Constr. Build. Mater. 30 (2012) 400–405. https://doi.org/10.1016/j.conbuildmat.2011.12.017.
[20] H. Javadian, F. Ghorbani, H. Tayebi, S.H. Asl, Study of the adsorption of Cd (II) from aqueous solution using zeolite-based geopolymer, synthesized from coal fly ash; kinetic, isotherm and thermodynamic studies, Arab. J. Chem. 8 (2015) 837–849. https://doi.org/10.1016/J.ARABJC.2013.02.018.
[21] Y. Li, P. Bai, Y. Yan, W. Yan, W. Shi, R. Xu, Removal of Zn 2+ , Pb 2+ , Cd 2+ , and Cu 2+ from aqueous solution by synthetic clinoptilolite, Microporous Mesoporous Mater. (2019). https://doi.org/10.1016/j.micromeso.2018.07.010.
[22] C.S. Cundy*, P.A. Cox, The Hydrothermal Synthesis of Zeolites: History and Development from the Earliest Days to the Present Time, Chem Rev. 103 (2003) 663–702. https://doi.org/10.1021/CR020060I.
[23] C.S. Cundy, P.A. Cox, The hydrothermal synthesis of zeolites: Precursors, intermediates and reaction mechanism, Microporous Mesoporous Mater. 82 (2005) 1–78. https://doi.org/10.1016/J.MICROMESO.2005.02.016.
[24] L. Gómez-Hortigüela, M.Á. Camblor, Introduction to the Zeolite Structure-Directing Phenomenon by Organic Species: General Aspects, in: Struct. Bond., Springer, Berlin, Heidelberg, 2017: pp. 193–223. https://doi.org/10.1007/430_2017_8.
[25] M.E. Davis, R.F. Lobo, Zeolite amd Molecular Sieve Synthesis, Chem. Mater. 4 (1992) 756–768.
[26] C. Amrhein, G.H. Haghnia, T.S. Kim, P.A. Mosher, T. Amanios, L. DelaTorre, Synthesis and properties of zeolites from coal fly ash, Environ. Sci. Technol. 30 (1996) 735–742. https://doi.org/10.1021/es940482c.
[27] M.A. Carreon, S. Li, J.L. Falconer, R.D. Noble, SAPO-34 seeds and membranes prepared using multiple structure directing agents, Adv. Mater. 20 (2008) 729–732. https://doi.org/10.1002/adma.200701280.
[28] E.M. Gallego, C. Paris, M.R. Díaz-Rey, M.E. Martínez-Armero, J. Martínez-Triguero, C. Martínez, M. Moliner, A. Corma, Simple organic structure directing agents for synthesizing nanocrystalline zeolites, Chem Sci. (2017). https://doi.org/10.1039/C7SC02858J.
[29] S.L. Burkett, M.E. Davis, Mechanism of Structure Direction in the Synthesis of Pure-Silica Zeolites. 2. Hydrophobic Hydration and Structural Specificity, Chem. Mater. 7 (1995) 1453–1463. https://doi.org/10.1021/cm00056a009.
[30] F.-S. Xiao, X. Meng, Zeolites in Sustainable Chemistry, Springer, 2016.

[31] A. Olivas, C.F. Ferraris, W. Guthrie, B. Toman, Re-Certification of SRM 2492: Bingham Paste Mixture for Rheological Measurements, Boulder, 2015.
[32] C.F. Ferraris, Measurement of the rheological properties of high performance concrete: State of the art report, J. Res. Natl. Inst. Stand. Technol. 104 (1999) 461. https://doi.org/10.6028/jres.104.028.
[33] I. Ismail, S.A. Bernal, J.L. Provis, S. Hamdan, J.S.J. Van Deventer, Drying-induced changes in the structure of alkali-activated pastes, J. Mater. Sci. 48 (2013) 3566–3577. https://doi.org/10.1007/s10853-013-7152-9.
[34] Z. Zhang, Y. Zhu, H. Zhu, Y. Zhang, J.L. Provis, H. Wang, Effect of drying procedures oaftn pore structure and phase evolution of alkali-activated cements, Cem. Concr. Compos. 96 (2019) 194–203. https://doi.org/10.1016/J.CEMCONCOMP.2018.12.003.
[35] G.W. Scherer, Effect of shrinkage on the modulus of silica gel, J. Non-Cryst. Solids. 109 (1989) 183–190. https://doi.org/10.1016/0022-3093(89)90030-6.
[36] A. Poulesquen, F. Frizon, D. Lambertin, Rheological behavior of alkali-activated metakaolin during geopolymerization, J. Non-Cryst. Solids. 357 (2011) 3565–3571. https://doi.org/10.1016/j.jnoncrysol.2011.07.013.
[37] A. Favier, J. Hot, G. Habert, N. Roussel, J.B. D'Espinose De Lacaillerie, Flow properties of MK-based geopolymer pastes. A comparative study with standard Portland cement pastes, Soft Matter. 10 (2014) 1134–1141. https://doi.org/10.1039/c3sm51889b.
[38] A. McCormick, A. Bell, C. Radke, Multinuclear NMR investigation of the formation of aluminosilicate anions, J. Phys. Chem. 93 (1989) 1741–1744.
[39] M. Criado, A. Fernández-Jiménez, A. Palomo, I. Sobrados, J. Sanz, Effect of the SiO2/Na2O ratio on the alkali activation of fly ash. Part II: 29Si MAS-NMR Survey, Microporous Mesoporous Mater. 109 (2008) 525–534. https://doi.org/10.1016/j.micromeso.2007.05.062.
[40] J.L. Provis, P. Duxson, G.C. Lukey, F. Separovic, W.M. Kriven, J.S.J. van Deventer, Modeling Speciation in Highly Concentrated Alkaline Silicate Solutions, Ind. Eng. Chem. Res. 44 (2005) 8899–8908. https://doi.org/10.1021/ie050700i.
[41] K.E. Jelfs, B. Slater, D.W. Lewis, D.J. Willock, The role of organic templates in controlling zeolite crystal morphology, in: Stud. Surf. Sci. Catal., Elsevier, 2007: pp. 1685–1692.
[42] R. Xu, J. Chen, Z. Gao, W. Yan, From Zeolites to Porous MOF Materials-the 40th Anniversary of International Zeolite Conference, 2 Vol Set: Proceedings of the 15th International Zeolite Conference, Beijing, PR China, 12-17th August 2007, Elsevier, 2007.
[43] C. Gittleman, K. Watanabe, A. Bell, C. Radke, A mechanistic study of the synthesis of zeolite SSZ-24, Microporous Mater. 6 (1996) 131–150.
[44] M. Romagnoli, C. Leonelli, E. Kamse, M. Lassinantti Gualtieri, Rheology of geopolymer by DOE approach, Constr. Build. Mater. 36 (2012) 251–258. https://doi.org/10.1016/j.conbuildmat.2012.04.122.
[45] W.H. Baur, On the cation and water positions in faujasite, Am. Mineral. J. Earth Planet. Mater. 49 (1964) 697–704.
[46] M. Calligaris, G. Nardin, L. Randaccio, Cation site location in hydrated chabazites. Crystal structure of potassium-and silver-exchanged chabazites, Zeolites. 3 (1983) 205–208.
[47] J. Felsche, S. Luger, C. Baerlocher, Crystal structures of the hydro-sodalite Na6 [AlSiO4] 6 8H2O and of the anhydrous sodalite Na6 [AlSiO4] 6, Zeolites. 6 (1986) 367–372.
[48] Y. Ji, Y. Wang, B. Xie, F.S. Xiao, Zeolite Seeds: Third Type of Structure Directing Agents in the Synthesis of Zeolites, Comments Inorg. Chem. 36 (2016) 1–16. https://doi.org/10.1080/02603594.2015.1031375.

[49] S.L. Burkett, M.E. Davis, Mechanism of Structure Direction in the Synthesis of Si-ZSM-5 : An Investigation by Intermolecular 1H-29Si CP MAS NMR Mechanism of Structure Direction in the Synthesis of Si-ZSM-5 : An Investigation by Intermolecular 1H-29Si CP MAS NMR, J. Phys. Chem. 98 (1994) 4647–4653. https://doi.org/10.1021/j100068a027.
[50] C.R.A. Catlow, D.S. Coombes, D.W. Lewis, J.C.G. Pereira, Computer Modeling of Nucleation, Growth, and Templating in Hydrothermal Synthesis, Chem. Mater. 10 (1998) 3249–3265. https://doi.org/10.1021/cm980302o.
[51] M. Jorge, S.M. Auerbach, P.A. Monson, Modeling spontaneous formation of precursor nanoparticles in clear-solution zeolite synthesis, in: AIChE Annu. Meet. Conf. Proc., American Chemical Society, 2005: p. 13926. https://doi.org/10.1021/JA052402I.
[52] R. Lloyd, Accelerated ageing of geopolymers, in: Geopolymers, Elsevier, 2009: pp. 139–166.
[53] M. Moliner, F. Rey, A. Corma, Towards the Rational Design of Efficient Organic Structure-Directing Agents for Zeolite Synthesis, Angew. Chem. Int. Ed. 52 (2013) 13880–13889.
[54] M. Criado, A. Fernández-Jiménez, A. Palomo, Alkali activation of fly ash. Part III: Effect of curing conditions on reaction and its graphical description, Fuel. 89 (2010) 3185–3192.
[55] A.V. McCormick, A.T. Bell, C.J. Radke, Quantitative determination of siliceous species in sodium silicate solutions by 29Si n.m.r. spectroscopy, Zeolites. 7 (1987) 183–190. https://doi.org/10.1016/0144-2449(87)90048-0.
[56] N.D. Hould, A. Foster, R.F. Lobo, Zeolite beta mechanisms of nucleation and growth, Microporous Mesoporous Mater. 142 (2011) 104–115. https://doi.org/10.1016/j.micromeso.2010.11.024.
[57] S.I. Zones, Conversion of faujasites to high-silica chabazite SSZ-13 in the presence of N,N,N-trimethyl-1-adamantammonium iodide, J. Chem. Soc. Faraday Trans. 87 (1991) 3709–3716. https://doi.org/10.1039/FT9918703709.
[58] S.I. Zones, S. Hwang, M.E. Davis, Studies of the Synthesis of SSZ-25 Zeolite in a “Mixed-Template” System, Chem. – Eur. J. 7 (2001) 1990–2001. https://doi.org/10.1002/1521-3765(20010504)7:9<1990::AID-CHEM1990>3.0.CO;2-G.
[59] X. Chen, A. Sutrisno, L. Zhu, L.J. Struble, Setting and nanostructural evolution of metakaolin geopolymer, J. Am. Ceram. Soc. 100 (2017) 2285–2295. https://doi.org/10.1111/jace.14641.
[60] P. Suraneni, S. Puligilla, E.H. Kim, X. Chen, L.J. Struble, P. Mondal, R. Suraneni, Monitoring Setting of Geopolymers, Adv. Civ. Eng. Mater. 3 (2014) 177–192. https://doi.org/10.1520/ACEM20130100.
[61] M. Mastali, P. Kinnunen, A. Dalvand, R. Mohammadi Firouz, M. Illikainen, Drying shrinkage in alkali-activated binders – A critical review, Constr. Build. Mater. 190 (2018) 533–550. https://doi.org/10.1016/j.conbuildmat.2018.09.125.
[62] J. Osio-Norgaard, W. V. Srubar, Zeolite Adsorption of Chloride from a Synthetic Alkali-Activated Cement Pore Solution, Materials. 12 (2019) 2019. https://doi.org/10.3390/ma12122019.
[63] J.F. Thompson, C. Bellerjeau, G. Marinick, J. Osio-Norgaard, A. Evans, P. Carry, R.A. Street, C. Petit, G.L. Whiting, Intrinsic Thermal Desorption in a 3D Printed Multifunctional Composite CO_2 Sorbent with Embedded Heating Capability, ACS Appl. Mater. Interfaces. (2019) acsami.9b14111. https://doi.org/10.1021/acsami.9b14111.